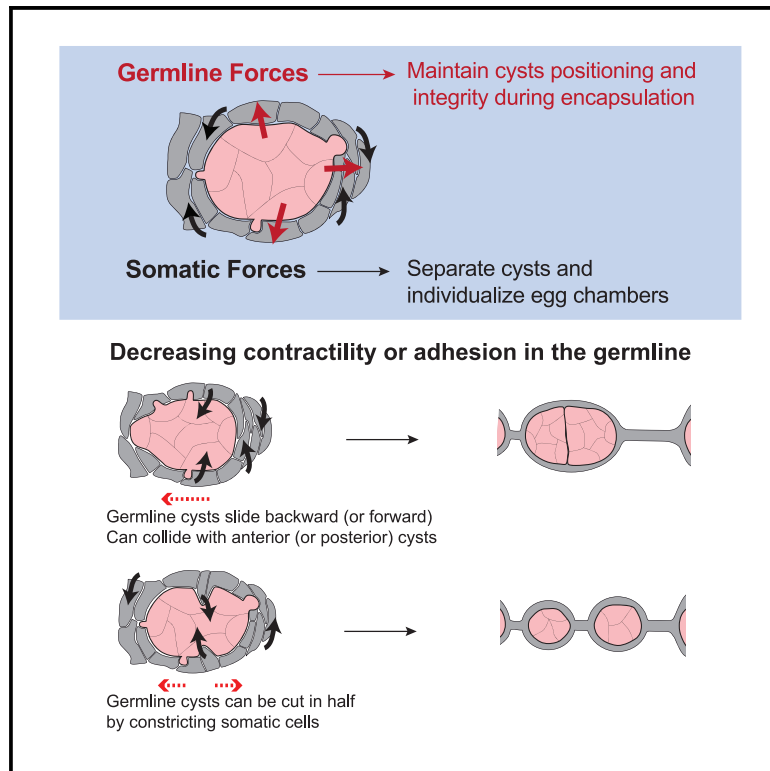


Collective Cell Sorting Requires Contractile Cortical Waves in Germline Cells

Graphical Abstract



Authors

Soline Chanut, Jean-René Huynh

Correspondence

jean-rene.huynh@college-de-france.fr

In Brief

Germline cysts generate contraction waves at the time of their encapsulation by somatic cells. Altering germ cell contractility or their adhesion to somatic cells induces encapsulation defects. Chanut and Huynh show that germ cells actively generate and transmit mechanical forces to maintain cyst integrity and positioning during encapsulation.

Highlights

- Germline cysts display contractile actomyosin waves at the time of encapsulation
- Altering contractility in germline cysts leads to encapsulation defects
- Germline cells generate mechanical forces to resist somatic constriction forces
- Germ cells actively maintain cyst integrity and positioning during encapsulation

Article

Collective Cell Sorting Requires Contractile Cortical Waves in Germline Cells

Soline Chanet¹ and Jean-René Huynh^{1,2,*}

¹Center for Interdisciplinary Research in Biology, Collège de France, PSL Research University, CNRS/UMR 7241 - INSERM U1050, 11 Place Marcelin Berthelot, 75005 Paris, France

²Lead Contact

*Correspondence: jean-rene.huynh@college-de-france.fr

<https://doi.org/10.1016/j.cub.2020.08.045>

SUMMARY

Encapsulation of germline cells by layers of somatic cells forms the basic unit of female reproduction called primordial follicles in mammals and egg chambers in *Drosophila*. How germline and somatic tissues are coordinated for the morphogenesis of each separated unit remains poorly understood. Here, using improved live imaging of *Drosophila* ovaries, we uncovered periodic actomyosin waves at the cortex of germ cells. These contractile waves are associated with pressure release blebs, which project from germ cells into somatic cells. We demonstrate that these cortical activities, together with cadherin-based adhesion, are required to sort each germline cyst as one collective unit. Genetic perturbations of cortical contractility, bleb protrusion, or adhesion between germline and somatic cells induced encapsulation defects resulting from failures to encapsulate any germ cells, or the inclusion of too many germ cells per egg chamber, or even the mechanical split of germline cysts. Live-imaging experiments revealed that reducing contractility or adhesion in the germline reduced the stiffness of germline cysts and their proper anchoring to the somatic cells. Germline cysts can then be squeezed and passively pushed by constricting surrounding somatic cells, resulting in cyst splitting and cyst collisions during encapsulation. Increasing germline cysts activity or blocking somatic cell constriction movements can reveal active forward migration of germline cysts. Our results show that germ cells play an active role in physical coupling with somatic cells to produce the female gamete.

INTRODUCTION

During development, tissues from different origins often cooperate and coordinate their morphogenetic movements to generate complex organs. Formation of the female gamete, for example, requires tight coordination between germ cells and the surrounding somatic tissue. During their differentiation, germ cells undergo several rounds of mitosis before entering meiosis. In most species, these mitoses are incomplete, giving rise to cysts of cells interconnected by cytoplasmic bridges [1]. Each germline cyst is then surrounded by cells of somatic origin called pre-granulosa cells in mammals and follicle cells (FCs) in *Drosophila* [2]. In mammals, pre-granulosa cells invade in between germ cells, and each cyst eventually breaks down (CBD) into single cells encased by granulosa cells, forming primordial follicles (PFs) [3]. In *Drosophila*, egg chambers are made of precisely 16 germ cells surrounded by an epithelium of FCs [4]. FCs do not invade the germline, and intercellular bridges are maintained throughout oogenesis. Encapsulation is a conserved and important process to investigate, as PFs and egg chambers give rise to the future female gamete, and encapsulation defects lead to sterility. Studies on the role of somatic cells during this step revealed general principles of epithelial morphogenesis [5–8]. In contrast, the contribution of germ cells to encapsulation remains poorly characterized, and germ cells are assumed to be passive, transported by somatic cells.

In *Drosophila*, these early steps of oogenesis take place in a specialized structure called the germarium at the anterior tip of the ovary (Figure 1A) [9]. The germarium contains both germline and somatic stem cells, which divide and assemble to produce egg chambers throughout adult life. Germline stem cells (GSCs) are located at the most anterior tip of region 1 of the germarium and give rise to cystoblasts. Cystoblasts then undergo 4 rounds of incomplete mitosis to generate cysts of 16 cells interconnected by ring canals. Only 1 cell per cyst becomes an oocyte; the remaining 15 cells differentiate as nurse cells. Once made of 16 cells, germline cysts enter region 2a, where they come into contact with FCs of somatic origin produced by follicle stem cells (FSCs) [10, 11]. This is when encapsulation starts. The 16 cells of each cyst become separated from other cysts by ingressing FCs that migrate centripetally [5, 12]. In region 2b, cysts flatten to take the shape of a disc spanning the width of the germarium. Moving posteriorly to region 3 (also known as stage 1), cysts increase in volume and become round again, encased by a monolayer of ~30 epithelial FCs. FCs at both poles of the cyst intercalate and form stalks of cells, which pinch off the newly formed egg chamber from the germarium into the vitellarium [12].

How the morphogenetic movements of encapsulation are coordinated between germ cells and somatic cells is not known. Mechanical forces that shape cells and tissue are usually produced by actomyosin contractility, in which the molecular motor

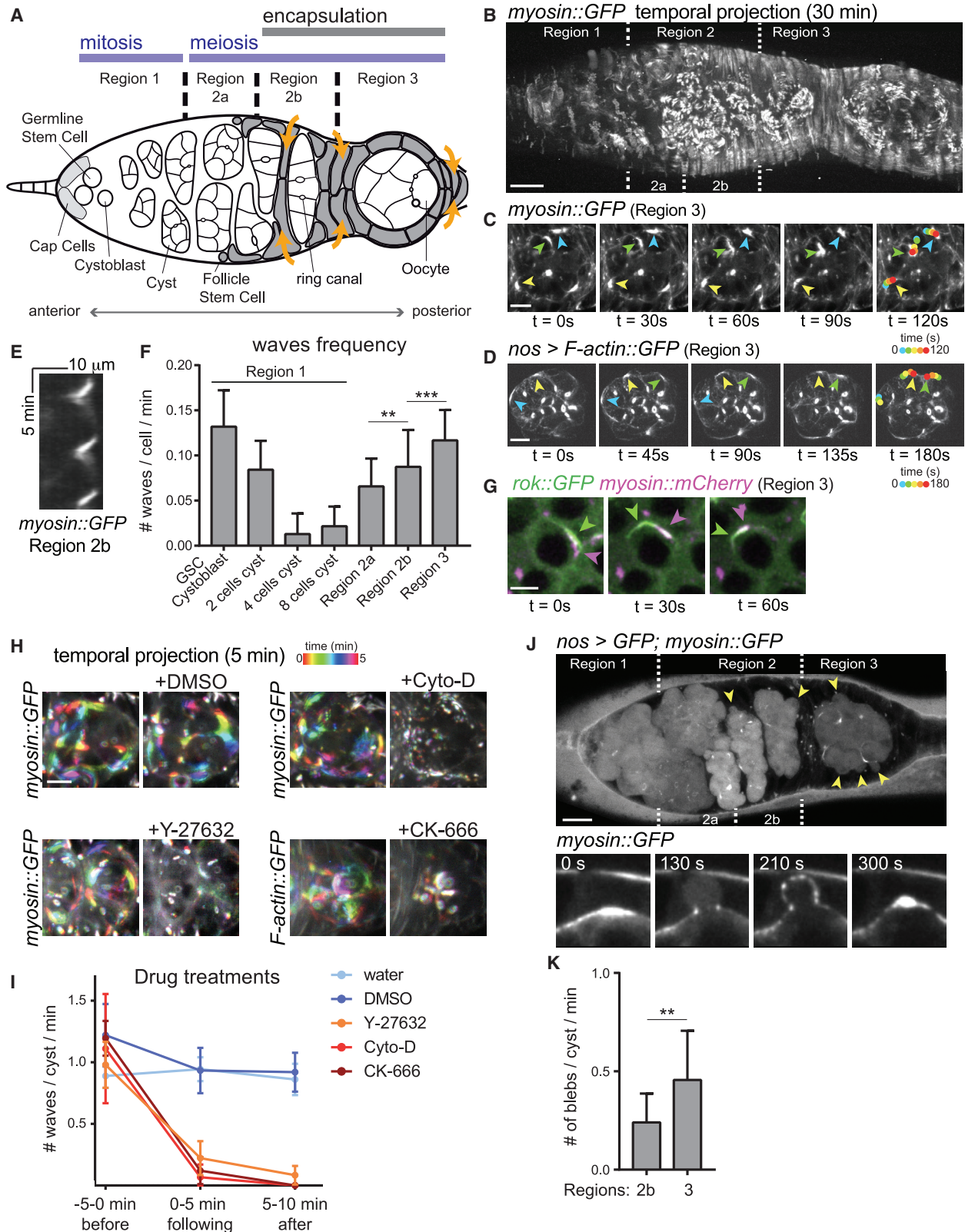


Figure 1. Germ Cells Generate Actomyosin Traveling Waves Associated with Pressure-Released Blebs

(A) The germline is divided into 4 morphological regions. Encapsulation takes place in regions 2b and 3 when FCs (gray) surround and separate germline cysts (orange arrows).

(legend continued on next page)

myosin II contracts cortical filamentous actin (F-actin). To be effective, these contractile forces must be transmitted to the extracellular substrate or neighboring cells through links between the F-actin network and junctional complexes, such as cadherins and integrins [13, 14]. In both mammals and flies, cadherins rather than integrins mediate interactions between somatic and germ cells at these early stages [8, 15].

In this study, we used hydrogel-based live imaging, genetics, and image analyses to investigate the role of germ cells during encapsulation. We show that germline cysts actively generate forces to maintain their position in the germarium while being surrounded by FCs and to preserve their integrity as groups of 16 cells.

RESULTS

Germ Cells Generate Actomyosin Traveling Waves

To investigate a potential role of germ cells during encapsulation, we looked at actomyosin dynamics in the germline. We observed waves of myosin and F-actin at the cortex of germline cysts (Figures 1B–1E; Video S1). The frequency of these waves was not uniform across the germarium and varied according to cyst differentiation. It was more periodic and intense in regions 2 and 3 (during encapsulation) than in region 1 (Figures 1B and 1F). In regions 2b and 3, we measured periods of the waves of 13.5 ± 1.2 min and 9.4 ± 0.5 min, respectively. We found that *myosin::Dendra2* photoconverted on one side of a cell could travel to the opposite side, demonstrating that myosin was traveling at an average speed of $0.028 \pm 0.0022 \mu\text{m s}^{-1}$ (Figure S1A) [16].

We next asked what regulates actomyosin waves. Myosin activation often occurs downstream of RhoA and its effector, the myosin-activating kinase ROCK (*rok* in *Drosophila*) [17, 18]. We observed that ROCK also traveled as waves at the cortex of germ cells, but slightly ahead of myosin waves (Figure 1G; the time shift between ROCK and myosin waves was ~ 30 s). To test whether the activity of ROCK was required for the propagation of these waves, we made use of the chemical inhibitor Y-27632. We used a water-based environment to be able to add this drug while recording. We adapted a live-imaging setup based on a photo-crosslinked polyethylene glycol (PEG) hydrogel, which could gently immobilize and maintain germarium morphology, while allowing the diffusion of aqueous medium and drug treatments (Figure S1B) [19]. The addition of Y-27632

stopped wave propagation within 1–2 min (Figures 1H and 1I; Video S2, A), while the addition of water alone had no effect (Figure 1I), indicating that ROCK activity was required for wave propagation. Next, we tested the requirement for F-actin dynamics. We found that adding cytochalasin D (Cyto-D), an inhibitor of actin turnover, or CK-666, which inhibits Arp2/3 and actin branching, completely repressed wave propagation. In contrast, we found that the addition of Colcemid, an inhibitor of microtubule polymerization, or DMSO alone had no effect on actomyosin wave dynamics (Figures 1H and 1I; Video S2).

These results describe periodic oscillations of the actomyosin cytoskeleton at the cortex of germline cells and demonstrate that wave propagation requires myosin activity and actin polymerization.

Cortical Contractility in Germ Cells Is Associated with Pressure-Release Blebs

Strong contractions of the actomyosin network can induce ruptures of the cortex or its detachment from the plasma membrane [20, 21]. These ruptures lead to the formation of cytoplasmic protrusions, called blebs, which release cytoplasmic hydrostatic pressure. The actomyosin meshwork then reforms inside the protrusion, driving bleb retraction. Blebs can thus be signs of strong cortical contractility. We observed that germline cysts were blebbing (Figure 1J; Video S3, A). When a bleb formed, it was preceded (within 1 min) by a cortical actomyosin wave in 48% of the cases ($n = 83$ blebs in 9 cysts from 4 germaria). In the remaining 52% of the cases, blebs formed at previous blebbing sites, where blebs already expanded and retracted. Inhibiting cortical contractility by adding Y-27632 or Cyto-D immediately eliminated blebs (Video S3, B). This showed that bleb formation in germ cells was dependent on actomyosin contractility. We found that bleb frequency followed the increase in wave occurrences from region 2b to region 3 (Figure 1K). We concluded that oscillations of actomyosin at the germ cells cortex were contractile and associated with blebs.

Alterations of Cortical Contractility in Germ Cells Lead to the Packaging of Abnormal Numbers of Germ Cells

To test the functional significance of contraction waves, we reduced cortical contractility in the germline, either by knocking down *chickadee* (*chic-RNAi*), the *Drosophila* homolog of profilin, required for actin polymerization, or *zipper* (*zip-RNAi*), which

(B) Temporal projection of a 30-min video (one z stack taken every 30 s) of a germarium expressing *sqh::GFP* that stains myosin.

(C and D) Time-lapse images (maximal z projection) of germline cysts in region 3 showing myosin (C) and actin (D) traveling waves around the cell cortexes. In the last images, wave displacement is represented with time-colored dots.

(E) Kymograph showing 3 consecutive waves of *sqh::GFP* (myosin) around the cortex of 1 cell from a cyst in region 2b. Frame rate, 20 s.

(F) Quantification of wave frequency depending on the developmental time of germline cyst cells. ** $p < 0.01$ and *** $p < 0.001$, t test.

(G) Time-lapse images of a germ cell expressing both *rok::GFP* (green) and *sqh::mCherry* (myosin, magenta). Green and magenta arrows point to the position (center) of *rok* and myosin waves, respectively.

(H) Temporal projection of 5-min movies of germline cysts in region 3 before (left) or after (right) drug or vehicle addition to the medium, as indicated. Time is color-coded, such that a rainbow signal indicates a traveling wave. Myosin (*sqh::GFP*) or F-actin (*utr::GFP*) waves are examined.

(I) Quantification of wave frequency per cyst in regions 2b or 3 before and after drug or vehicle treatments. Means and standard deviations (SDs) are shown. $n = 4$ germaria treated with water, $n = 5$ germaria treated with DMSO, $n = 6$ germaria treated with Y27632, $n = 6$ germaria treated with Cyto-D, $n = 5$ germaria treated with CK-666.

(J) Cytoplasmic expression of GFP in the germline reveals the presence of bleb protrusions (top, arrows). Still images following a bleb formation and retraction (bottom).

(K) Quantification of bleb frequency per cyst in regions 2b and 3. Means and SDs are shown. ** $p < 0.01$, t test.

Scale bars, 10 μm (B and J) and 5 μm (C, D, G, and H).

See also Videos S1, S2, and S3 and Figure S1.

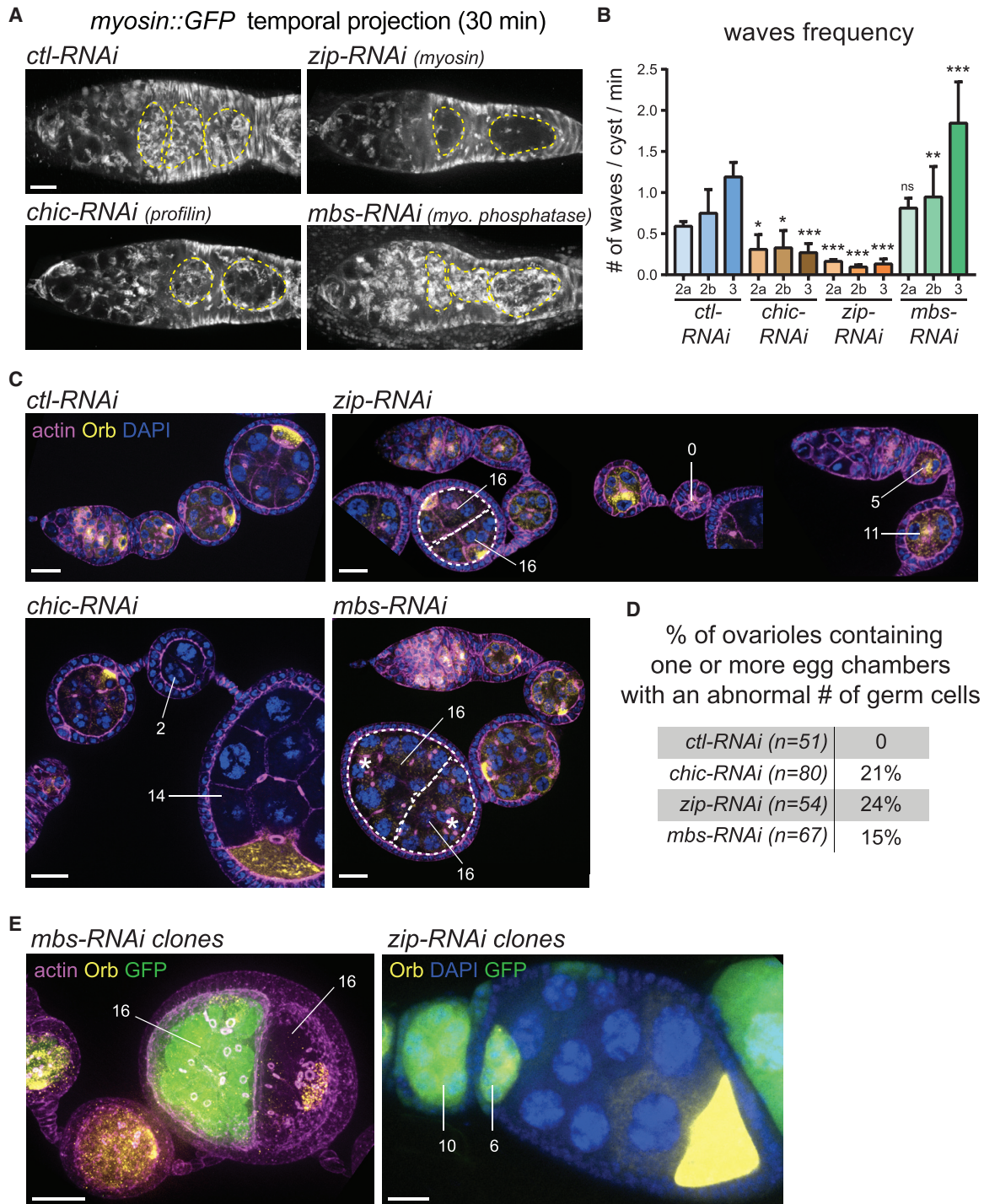


Figure 2. Alteration of Germline Contractility Induces the Formation of Abnormal Egg Chambers

(A) Temporal projection of 30-min videos (1 z stack taken every 30 s) of germlaria expressing *sqh::GFP* to follow myosin waves in the indicated mutant conditions. Germline cysts are outlined with yellow dotted lines.

(B) Quantification of wave frequency per cyst in regions 2 and 3 of the germlarium. Indicated RNAi were expressed specifically in the germline. Means and SDs are shown. * $p < 0.05$, ** $p < 0.01$, *** $p < 0.001$; ns, not significant, t test.

(C) Fixed images of ovarioles stained with phalloidin (actin, magenta), Orb (oocyte, yellow), and DAPI (blue). White dotted lines show 2 different cysts packaged together in 1 egg chamber. Numbers indicate the number of germ cells included in each unit. Asterisks mark the position of the 2 oocytes of the 2 *mbs-RNAi* cysts.

(D) Quantification of the occurrence of phenotypes in fixed ovarioles for different mutant conditions.

(legend continued on next page)

encodes for myosin II heavy chain. Depleting *chic* or *zip* in germ cells effectively reduced cortical myosin intensity and wave frequency compared to a control knocked down (*ctl-RNAi*) (Figures 2A and 2B, Video S4). We obtained a similar reduction in cortical contractility in germline cysts mutant for ROCK (*rok²*) (Figure S2A). We also tested the consequences of increasing cortical contractility by inhibiting *mbs*, the myosin-binding subunit of the myosin phosphatase, which dephosphorylates and inhibits myosin. Depleting *mbs* in the germline (*mbs-RNAi*) increased wave frequency and blebbing (Figures 2A, 2B, and S2C; Video S4).

The most striking phenotype induced by both reducing and increasing contraction waves in the germline was the observation of egg chambers containing an abnormal number of germ cells (Figures 2C and 2D). Instead of egg chambers containing 16 germ cells with 1 oocyte, mutant egg chambers were made of a number of germ cells ranging from 0 to 32 cells, with 0, 1, or 2 oocytes (Figures 2C and 2D, oocyte marked by “Orb”). The abnormal number of germ cells could come from defects in the mitosis of single-cell precursors (abnormal number of divisions or defective abscission of GSCs/cystoblasts) [22, 23] or from defects in cell sorting, with the encapsulation of germ cells from different cysts into the same egg chamber. To distinguish between these two hypotheses, we performed a cell-lineage analysis to label germline cysts generated by a single-cell precursor. In our experiment, RNAi-expressing cysts were GFP⁺ and wild-type cysts were GFP⁻. The observation that a single egg chamber can contain 1 group of 16 GFP⁺ cells and a distinct group of 16 GFP⁻ cells indicated that egg chambers containing 32 germ cells comprise 2 different 16-cell cysts packed together (Figure 2E) and not a single 32-cell cyst caused by abnormal divisions. Similar results were obtained with germline clones mutant for *sqh¹* (myosin mutant; Figure S2B). We also found that egg chambers with <16 germ cells were associated with neighboring egg chambers containing the missing complement of GFP⁺ germ cells (Figure 2E; 10 GFP⁺ germ cells in 1 egg chamber are associated with the missing 6 GFP⁺ germ cells in the neighboring egg chamber). The last category of phenotypes was the presence of long stalks of FCs that sometimes formed a ball or a pseudo-egg chamber empty of any germ cells (Figure 2C).

We concluded that altering the cortical contractility induced defects in sorting germline cysts into groups of 16 cells and resulted in the formation of unfertile egg chambers with abnormal numbers of germ cells.

Abnormal Number of Germ Cells in Contractility Mutants Are Caused by Encapsulation Defects

To test whether abnormal egg chambers originated from encapsulation defects, we live imaged the early steps of encapsulation in a hydrogel. We followed the displacement of individual cysts along the anterior-posterior (a-p) axis, at the time the cysts started to be separated by FCs (in regions 2b and 3 of the

germarium). In *ctl-RNAi* conditions, we observed that when somatic cells ingressed to separate 2 cysts, the older cyst (in region 3) was slightly displaced toward the posterior of the germarium (positive orientation in Figure 3B), and the younger cyst (in region 2b) was slightly displaced toward the anterior (negative orientation in Figure 3B) (Figures 3A and 3B, Video S5, A). Overall cyst displacement was small; we measured a mean displacement speed of $0.0125 \pm 0.0019 \mu\text{m min}^{-1}$, which is in accordance with previous recordings of wild-type cyst movements [12].

In *chic-RNAi* and *zip-RNAi* conditions, however, cyst movements were significantly increased (Figure 3B; Video S5, B and C). Cysts in regions 2b and 3 were frequently pushed back together more anteriorly (Figure 3A, *zip-RNAi*, top). These increased movements resulted in collisions between cysts in the germarium and the formation of long stretches of FCs. If collisions were not resolved at the time of egg chamber individualization, then this would lead to the formation of a compound egg chamber containing two cysts packaged together.

In *chic-RNAi* and *zip-RNAi*, we also noticed that cysts in region 3, instead of being round, adopted an elongated shape along the a-p axis compared to controls (Figure 3C, increased aspect ratio). Live imaging showed cysts being squeezed and sometimes cut into several parts by ingressing FCs (Figure 3A, *zip-RNAi*, bottom; Video S5, B and C). Cyst-splitting events would give rise to egg chambers with <16 germ cells. In addition, different parts of the split cysts could be packaged with adjacent cysts generating egg chambers with >16 cells.

In *mbs-RNAi*, cyst movements and speed were also increased compared to control conditions. Whereas in *zip-RNAi* and *chic-RNAi* cysts tend to be more frequently pushed toward the anterior, *mbs-RNAi* cysts tend to move most frequently toward the posterior (Figure 3B). This behavior was more pronounced for cysts in region 3 that significantly moved faster toward the posterior than *ctl-RNAi*, and in the strongest instances, can collide with an older cyst, resulting in the encapsulation of the two cysts together (Video S5, C). In contrast to *chic-RNAi* and *zip-RNAi*, we never observed cysts being split in *mbs-RNAi*. *mbs-RNAi* cysts were not squeezed but remained round in region 3, with an aspect ratio close to 1 (Figure 3C). These results suggest that increasing cortical contractility in *mbs-RNAi* favors faster displacement of the cysts toward the posterior of the germarium.

Our live-imaging experiments showed that cortical contractility is required in germ cells to maintain the correct positioning of cysts at the time of encapsulation, to avoid both collisions between cysts and the formation of long stalks of FCs devoid of germ cells. Germline contractility is also required to confer stiffness to the cysts, maintaining their integrity as a group of 16 cells and avoiding cyst splitting. Thus, the alteration of cortical contractility in germ cells induced a loss of coordination between germline and somatic cell movements. Next, we looked for links between germ cells and somatic cells that could mediate this coordination.

(E) Fixed mosaic ovariole showing 1 GFP⁺ *mbs-RNAi* cyst packaged with an unmarked wild-type cyst within the same egg chamber (left). (Right) Fixed mosaic ovariole showing a GFP⁺ *zip-RNAi* cyst that is split between 2 egg chambers (numbers indicate the number of cells from the original cyst). Scale bars, 10 μm (A) and 20 μm (C and E).

See also Figure S2 and Video S4.

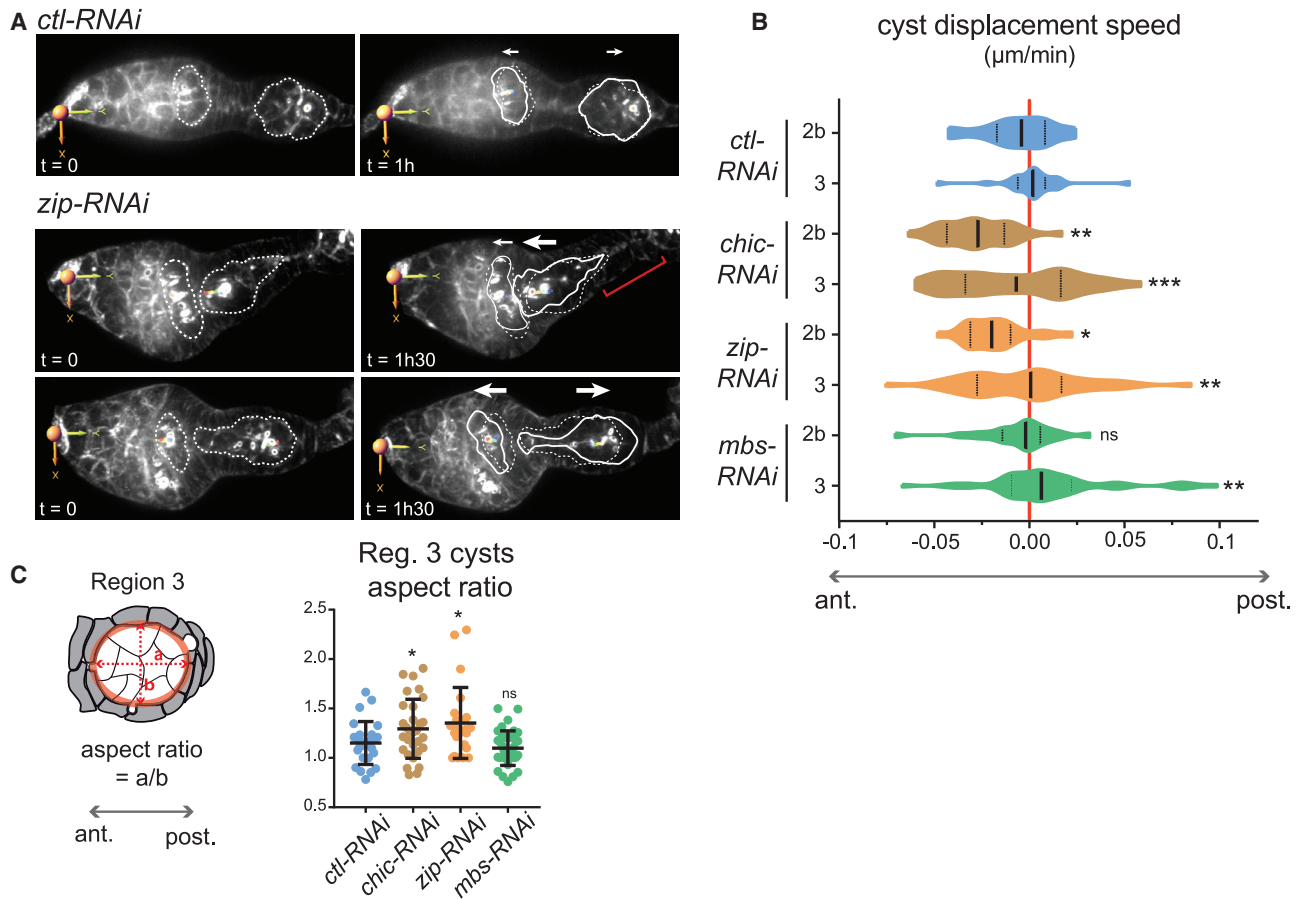


Figure 3. Alteration of Germline Contractility Leads to Defective Sorting during Encapsulation

(A) Still images from videos of *ctl-RNAi* and *zip-RNAi* germaria. Original (dashed lines) and final (solid lines) cyst positions are indicated. The white arrows indicate the cyst displacement direction. The red bracket indicates long stalk.

(B) Quantification of cyst displacement speed along the a-p axis in regions 2b and 3 of the germarium. Violin plots with median and 25%–75% quartiles are shown. * $p < 0.05$, ** $p < 0.01$, *** $p < 0.001$; ns, non-significant, Mann-Whitney U test (performed on absolute speed values).

(C) Schematic of a region 3 germline cyst surrounded by somatic cells. To measure the elongation of the cyst along the a-p axis, we measured the aspect ratio of the fitted ellipse (red) as illustrated (left). (Right) Quantification of the region 3 cyst aspect ratio. Dot and whisker plots are shown. * $p < 0.05$; ns, non-significant, t test.

See also Video S5.

Cadherin-Based Adhesion Is Required for Correct Encapsulation

During oogenesis, interactions between germ cells and somatic cells are mediated by E-cadherin (E-Cad) homophilic interactions [24, 25]. We also showed previously that adherens junctions are present between germ cells around ring canals (Figure 4A; Video S6) [26]. β -Catenin (*armadillo*, *arm* in *Drosophila*) and α -catenin link E-Cad to the underlying actomyosin cortex [7, 27, 28].

To decrease homophilic interactions between germ and somatic cells, we depleted E-Cad (*shotgun*, *shg* in *Drosophila*) either in the germline (*ECad-RNAi germ*, Figure S3A) or in the FCs (*ECad-RNAi soma*, Figure S3A). FCs also expressed N-cadherin (N-Cad, Figure S3B), which could maintain epithelial architecture after the depletion of E-Cad in the somatic layer. We found that depleting E-Cad induced encapsulation phenotypes, similar to those observed after *zip* or *chic* were knocked down in the germline. On fixed ovaries, we found egg

chambers made of two 16-cell cysts or separated by long empty stalks (Figures 4B and 4C). In addition, when E-Cad was depleted in the germline, we found a majority of egg chambers with fewer germ cells, indicating that groups of 16 cells had been split between several egg chambers (Figure 4B). As in *chic-RNAi* or *zip-RNAi*, occurrences of split cysts correlated with strong deformations of *ECad-RNAi germ* mutant cysts along the a-p axis in region 3 (Figure 4D). However, egg chambers containing split cysts were not observed when E-Cad was depleted in FCs only, and the cyst aspect ratio in region 3 was not affected in this case (Figure 4D).

Live imaging confirmed these encapsulation defects. We observed increased cyst movements in regions 2b and 3 of the germarium, with cysts being pushed toward the anterior or the posterior, leading to collisions with the preceding or following cyst (Figures 4E and 4F; Video S7, A and B). We also observed cysts being deformed along the a-p axis and split by FCs when E-Cad was knocked down in the germline (Video S7, C).

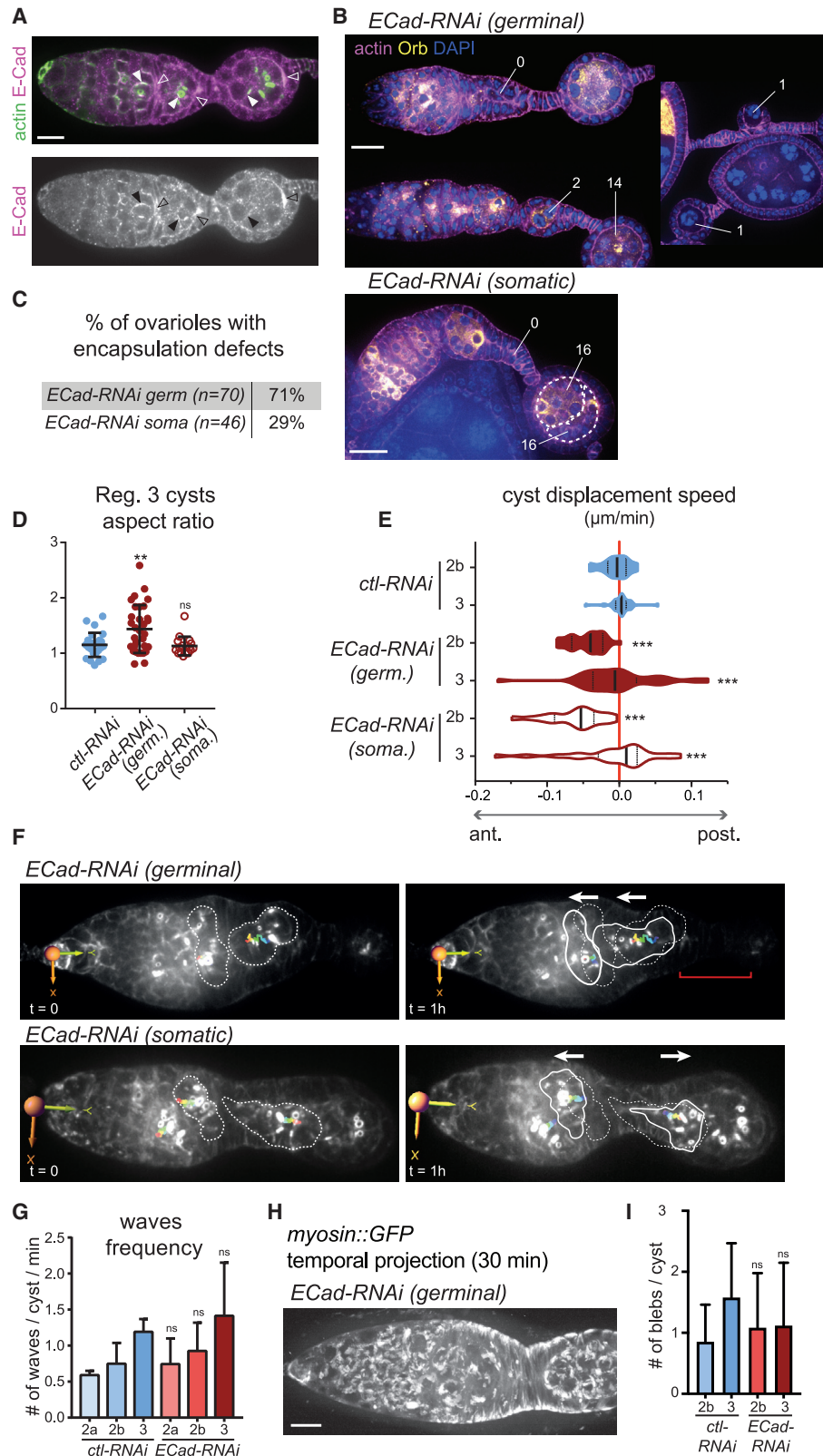


Figure 4. Cadherin-Based Adhesion Is Required for Correct Encapsulation

(A) Wild-type germline stained with E-Cad (magenta) and F-actin (green). E-Cad was localized within the germline cells around the ring canals (solid arrows) and between the germline cysts and the somatic layer (empty arrows).

(legend continued on next page)

Similar phenotypes were observed when inducing germline clones of a null allele of *E-Cad* (*shg^{R69}*) (Figure S3D; 62.5% of ovarioles with encapsulation defects, $n = 16$) or when knocking down *armadillo* in the germline (*arm-RNAi*, 12% of ovarioles with encapsulation defects, $n = 75$; Figure S3C; Video S7, D). In addition, encapsulation defects were reported with mutant alleles of β -catenin and α -catenin [7, 27, 28].

These results showed that reducing cell adhesion in either germ or somatic cells gave similar encapsulation phenotypes than did impairing the cortical contractility in germ cells. We thus tested whether reducing cell adhesion affected germline cell contractility. We found that neither wave frequency nor bleb occurrences were affected in *ECad-RNAi* mutant cysts (Figures 4G–4I; Video S4). Eliminating cell adhesion thus does not noticeably affect germ cell contractility.

We concluded that correct encapsulation requires the generation of contractile forces by germline cysts and adhesion between germ cells to prevent cyst splitting. It also requires the transmission of these contractile forces to FC layers through *E-Cad* adhesion complexes to maintain cyst position and proper cyst anchorage to somatic cells, preventing collisions between cysts.

Altering Bleb Frequency Leads to Encapsulation Defects

To manipulate bleb occurrences without directly affecting actomyosin activity, we thought of modifying properties of the cortex by expressing two different mutant forms of Moesin in germ cells. Moesin is a FERM-domain protein that links the actomyosin cortex to the plasma membrane. Its activity is regulated by phosphorylation at T559 [29]. We tested whether expressing a non-phosphorylatable or a phosphomimetic form of Moesin (*moe-TA::GFP* and *moe-TD::GFP*, respectively) affected overall cortical contractility. We found no differences in wave frequencies or cyst aspect ratios in region 3 when *moe-TA::GFP* or *moe-TD::GFP* was expressed in the germline compared to controls (Figures S4A and S4B), indicating that cortical actomyosin activity was not significantly altered in these contexts.

However, when we expressed *moe-TA::GFP* in germ cells, known for its dominant-negative function, we noticed an increase in the average number of blebs per cyst (Figures 5A and 5B). This correlated with encapsulation defects and the formation of egg chambers with abnormal numbers of germ cells (Figures 5C and 5D). Cell lineage analysis further showed that GFP⁺ cysts expressing *moe-TA::GFP* could be found packaged with a wild-type cyst in a compound egg chamber (Figure 5C).

We observed that *moe-TA::GFP*-overexpressing cysts in region 3 moved more and faster toward the posterior than did control cysts (Figure 5E). A highly blebbing cyst could sometimes contact and invade a posterior cyst, leading to cyst collision (Figure 5F; Video S8).

Expressing *moe-TD::GFP* in germ cells is thought to induce a stiffer cortex. We observed smaller blebs and a decrease in bleb numbers, although these were not statistically significant (Figures 5A and 5B). In contrast to cysts expressing *moe-TA::GFP*, cysts expressing *moe-TD::GFP* were not able to significantly move forward and only induced mild encapsulation defects (Figures 5D and 5E).

These results showed that blebs could play a role during encapsulation. Increasing bleb occurrences was sufficient to accelerate the movement of germline cysts, which can induce collisions and encapsulation defects.

Germline Cysts Play an Active Role in Cyst Sorting Using Migration-like Mechanisms

To reveal a putative germ cell autonomous role in cyst positioning during encapsulation, we aimed to block somatic cell movement and thus suppress constriction forces exerted on germline cysts. We did so by mechanically blocking the centripetal migration of FCs. We observed that when we mounted a germarium in halocarbon oil (10S), it tended to flatten on the coverslip to minimize contact with oil, the bottom surface of the germarium stuck to the coverslip, making FCs unable to move and migrate. In normal conditions, FC convergent-extension movements constrict the germarium in between cysts, progressively reducing the width of the stalk that will separate the future egg chambers (Figure 6A) [12]. In hydrogel, we measured a reduction in $4.5\% \pm 0.5\%$ of the stalk width in 50 min. In oil, FCs tended instead to slightly expand on the coverslip ($0.6\% \pm 1.0\%$ of the stalk width; Figure 6A). FCs were thus not able to intercalate and constrict the underlying germ cells. In these conditions, we measured a positive movement of germline cysts toward the posterior of the germarium, indicating that wild-type germline cysts were able to migrate on stalled FCs, which can lead to collision between cysts (Figures 6B and 6C; Video S9, A). Knockdown of *zip* or *E-Cad* in the germline, however, significantly reduced germline cyst movement and speed in germarium mounted in oil (Figure 6B). This indicated that the ability of cysts to migrate on stalled FCs depends on cortical contractility and adhesion with surrounding FCs. These results also revealed that fast displacement of germline cysts with reduced cortical contractility or adhesion observed in hydrogel was

(B) Fixed images of ovarioles stained with phalloidin (actin, magenta), Orb (oocyte, yellow), and DAPI (blue). The white dotted lines show 2 different cysts packaged together in 1 egg chamber. The numbers indicate the number of germ cells included in each unit.

(C) Quantification of the occurrence of encapsulation phenotypes in fixed ovarioles.

(D) Quantification of region 3 cyst aspect ratio. Dot and whisker plots are shown. ** $p < 0.01$; ns, not significant, t test.

(E) Quantification of cyst displacement speed along the a-p axis. Violin plots with medians and 25%–75% quartiles are shown. *** $p < 0.001$; Mann-Whitney *U* test (performed on absolute speed values).

(F) Still images from videos of *Ecad-RNAi germ* and *ECad-RNAi soma* germaria. The original (dashed lines) and final (solid lines) cyst positions are indicated. The white arrows indicate the cyst displacement direction. The red bracket indicates long stalk.

(G) Quantification of wave frequency per cyst in regions 2 and 3 of the germarium. Means and SDs are shown. ns, not significant, t test.

(H) Temporal projection of a 30-min video (1 z stack taken every 30 s) of a *ECad-RNAi* germarium.

(I) Quantification of the average number of blebs per cyst in regions 2b and 3. Means and SDs are shown. ns, not significant, t test.

Scale bars, 20 μm (A and B) and 10 μm (H).

See also Videos S4, S6, and S7 and Figure S3.

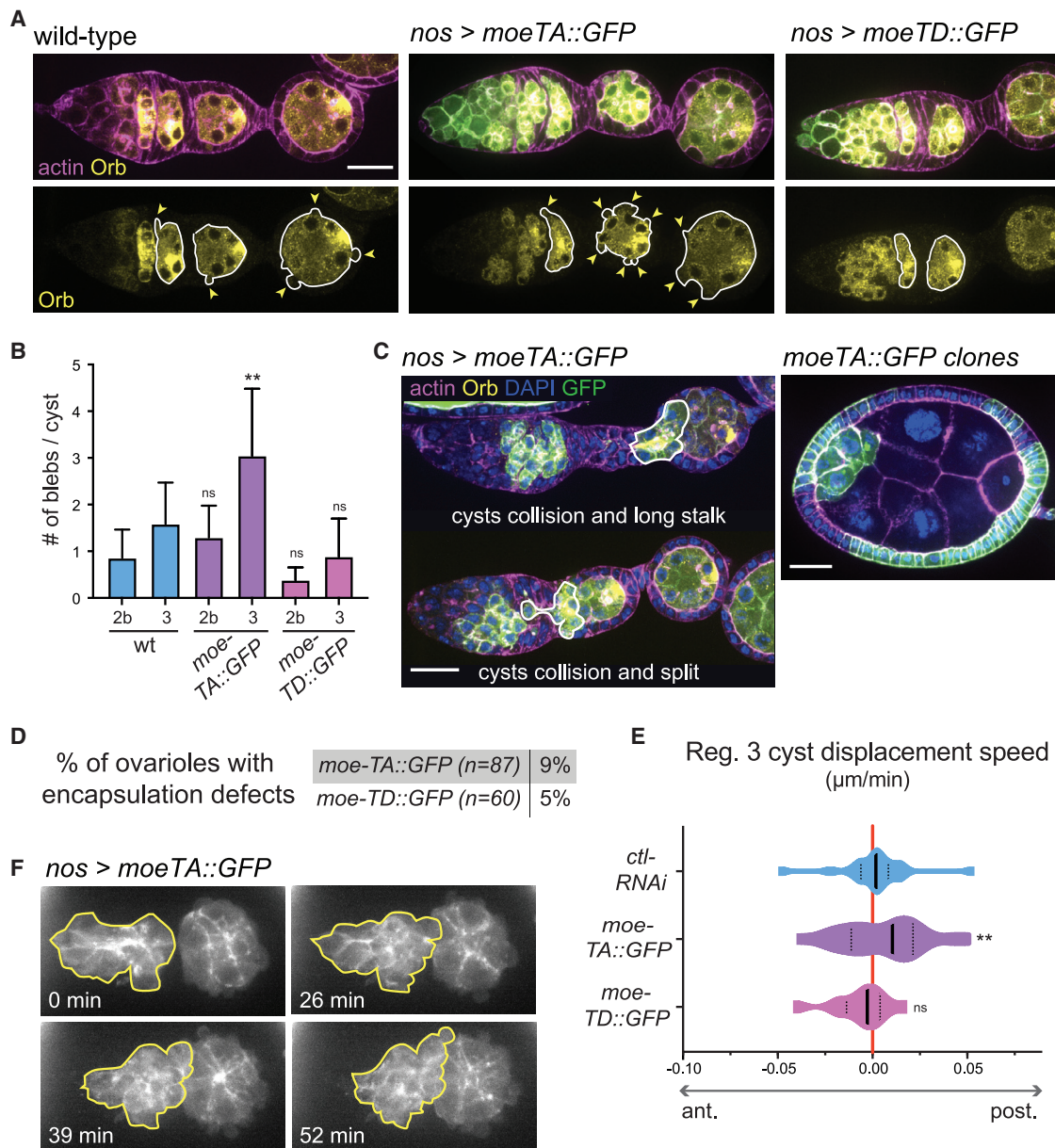


Figure 5. Increasing Bleb Frequency Induces Forward Movements of Germline Cysts and Cyst Collisions

(A) Wild-type germlarium (left) and germlaria overexpressing *moe-TA::GFP* or *moe-TD::GFP* in the germline (center and left) stained with Orb (oocyte, yellow) and phalloidin (actin, magenta). The cyst boundaries are marked with a white line. The blebs are indicated with arrows.

(B) Quantification of the average number of blebs per cyst in regions 2b and 3. Means and SDs are shown. ** $p < 0.001$; ns, non-significant, t test.

(C) Fixed images of ovarioles overexpressing *moe-TA::GFP* (green) stained with phalloidin (actin, magenta), Orb (oocyte, yellow), and DAPI (blue). (Left) Anterior cysts colliding with an older cyst are marked with a white line. (Right) Compound egg chamber made of a *moe-TA::GFP*-overexpressing cyst and 1 unmarked wild-type cyst.

(D) Quantification of the occurrence of encapsulation phenotypes in fixed ovarioles.

(E) Quantification of cyst displacement speed along the a-p axis. Only cysts in region 3 were considered. Violin plots with medians and 25%–75% quartiles are shown. ns, non-significant. ** $p < 0.01$; Mann-Whitney *U* test (performed on absolute speed values).

(F) Still images from a video of a germlarium overexpressing *moe-TA::GFP* in the germline. An anterior cyst (yellow outline) migrates forward and collides with a posterior cyst.

Scale bars, 20 μm.

See also [Video S8](#) and [Figure S4](#).

passive and imposed by surrounding FC constriction forces (Figures 3B and 4E). Mutant cysts were passively pushed backward or forward as somatic cells rearranged and constricted to

form a stalk (Figure S5A). We next followed cyst displacement when FC contractility and movements were genetically impaired. Knocking down *zip* in the FCs (*zip-RNAi soma*) led

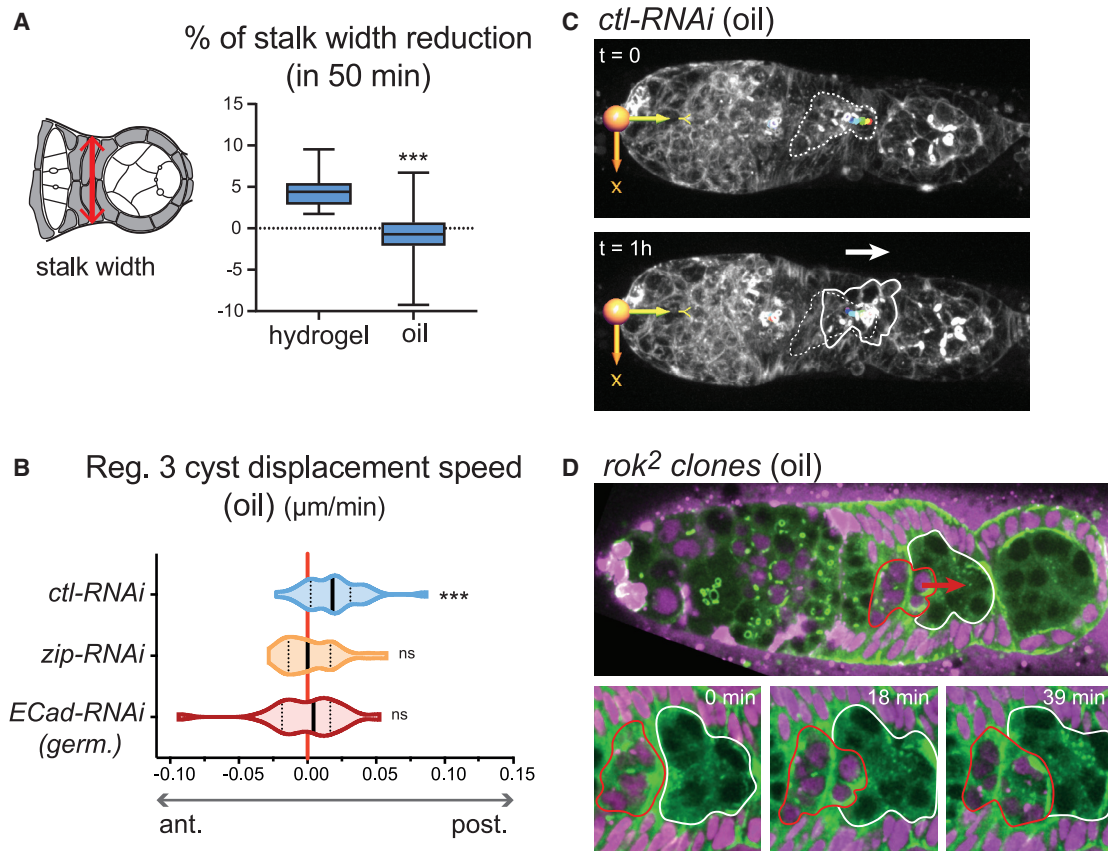


Figure 6. Germline Cysts Can Migrate When Somatic Cell Movement Is Blocked

(A) Schematic of the posterior part of the germarium (left). FCs form a stalk that separates the 2 cysts. The red arrow indicates where the stalk width was measured. (Right) Quantification of the percentage of stalk width reduction during 50 min of recording, for germaria mounted in either hydrogel or oil (negative values indicate expansion). Box and whisker plots are shown. *** $p < 0.001$, t test.

(B) Quantification of cyst displacement speed along the a-p axis when germaria are mounted in oil. Violin plots with medians and 25%–75% quartiles are shown. *** $p < 0.001$; ns, non-significant. One sample Wilcoxon signed rank test (test against the null hypothesis, $m = 0$, no displacement).

(C) Still images from a video of a control germarium (*ctl-RNAi*) mounted in oil. The original (dashed line) and final (solid line) cyst positions are indicated. The white arrow indicates the cyst displacement direction.

(D) Still images of a mosaic germarium containing wild-type (RFP⁺, magenta) germline cyst and *rok²* mutant cysts. High magnifications are shown. A wild-type cyst (RFP⁺, red outline) migrates forward and invades the position of a mutant cyst (unmarked, white outline). The red arrow indicates cyst displacement direction. See also [Video S9](#) and [Figure S5](#).

to the formation of long germaria containing multiple cysts that were not separated by somatic cells, indicating that their convergent-extension movements were inhibited. We followed the displacement of round cysts in *zip-RNAi soma* germaria mounted in hydrogel and measured positive movements of germline cysts toward the posterior, confirming that wild-type germline cysts were able to migrate on stalled FCs ([Figure S5B](#); [Video S9](#), B).

Thus, our data suggest that cortical contractility in germ cells can generate forces that enable cysts to migrate. To support this idea, we compared two populations of germline cysts within the same germarium using clonal analysis. We induced mosaic germaria containing germline cysts mutant for *rok* and marked by the absence of red fluorescent protein (RFP; wild-type cysts are RFP⁺) ([Figure 6D](#)). *rok* mutant cysts showed a clear reduction in wave frequency ([Figure S2A](#)). Under these conditions, wild-type cysts invaded posterior *rok* mutant cysts, indicating that wild-type cysts were consistently faster than *rok* mutant cysts

([Figure 6D](#); [Video S9](#), C). Consistently, we never detected the reverse invasion of wild-type cysts by mutant cysts ($n = 6$ invasions of *rok²* mutant cysts by wild-type cysts, 9 mosaic germaria).

These results suggest that in normal conditions, germline cysts use migration-like mechanisms to maintain their position within the germarium during encapsulation. Their autonomous movement toward the posterior is usually masked by the prominent movements and constriction of FCs around them that tend to push neighboring cysts in the opposite direction to separate them. However, if we mechanically or genetically block FC movements, then germline cysts can visibly migrate forward ([Figure 7](#)).

DISCUSSION

Our study revealed the existence of periodic contractile waves of the actomyosin network at the cortex of germ cells, as described

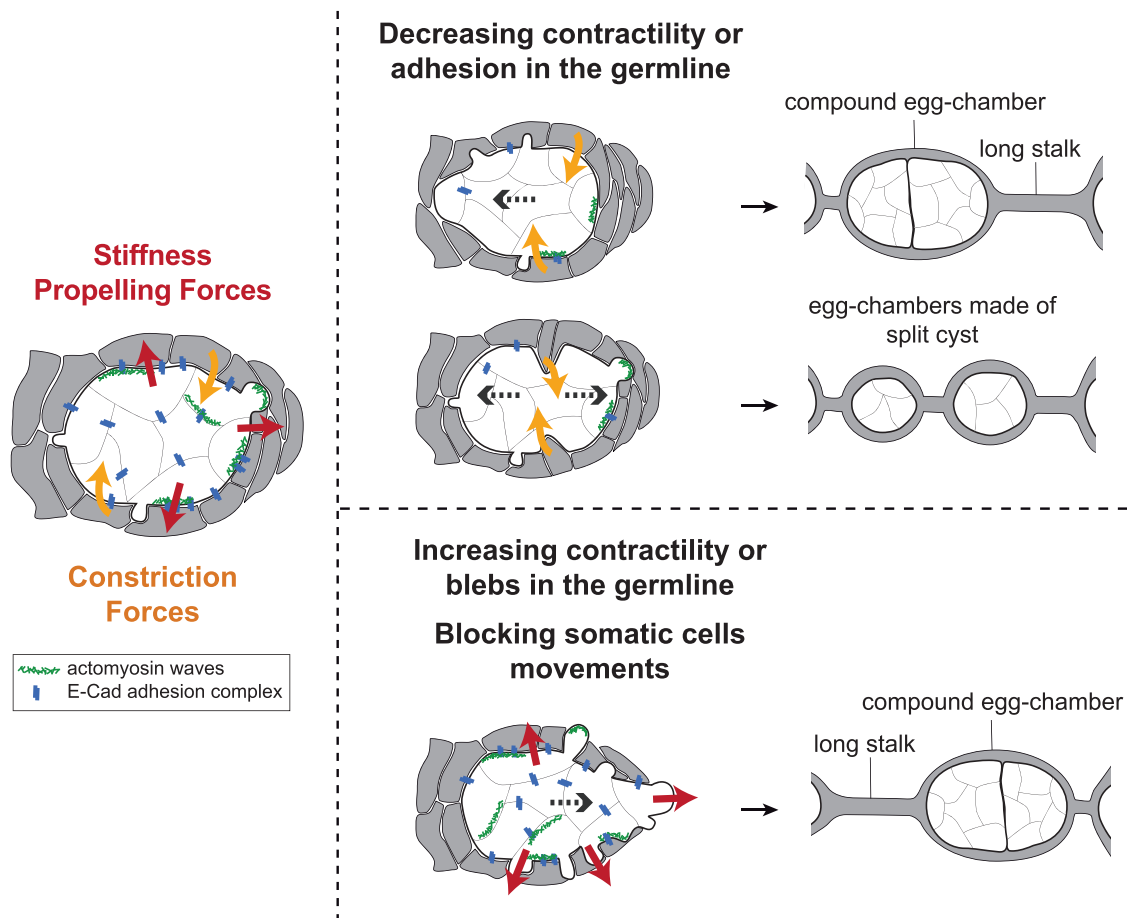


Figure 7. Encapsulation Requires a Proper Balance between Germline and Somatic Forces

(Left) Germline cysts exert mechanical forces dependent on cortical contractility and adhesion (red arrows). This confers stiffness within the 16-cell cyst to maintain cyst integrity and propelling forces to maintain the proper cyst positioning during encapsulation. At the same time, somatic cells migrate around germline cysts, exerting constriction forces (orange arrows). In the wild type, germline forces resist constriction forces exerted by surrounding somatic cells and maintain the correct cyst position during encapsulation.

(Right) Modifying the equilibrium between germline and somatic forces decouples cyst movement from somatic cells movement. On the one hand, decreasing germline contractility or adhesion induces germline cysts sliding backward or forward, leading to cyst collision, which can lead to the formation of compound egg chambers. Decreasing germline contractility or adhesion also induces cyst splitting by constricting somatic cells, which generates incomplete egg chambers. On the other hand, increasing germline contractility or blebbing or blocking somatic cell movement can induce a net forward migration of the germline cysts that can also result in cyst collision and encapsulation defects.

in other developmental systems [30–32]. We demonstrated that these contractions are required to maintain the correct anchorage and positioning of germline cysts during encapsulation by FCs and to maintain their integrity as groups of 16 cells. We propose that there are two kinds of forces at play during encapsulation (Figure 7). Convergent intercalation of somatic cells exerts constriction forces on the underlying germline cells, while contractility and protrusions of germ cells exert propelling forces on the overlying FCs. Correct encapsulation requires a proper balance between these forces. On the one hand, when the contractility of germ cells was weakened, somatic cells could squeeze and cut or displace germline cysts. On the other hand, when somatic cell convergence was blocked, germline cells could migrate on stalled FCs and collided.

We further showed that E-Cad-based adhesion between germline and somatic cells is required to transmit forces and to

coordinate both morphogenetic movements. Knocking down contractility in germ cells or cadherin-based adhesion between germline cysts and FCs both lead to increased and uncontrolled movements of germline cysts. Mechanistically, we propose that cortical contractility at the interface between germline cysts and FCs helps to remodel dynamically cellular adhesion. This may involve junctional strengthening under tension or contractility-dependent E-Cad turnover and junction remodeling [33–35]. In addition, friction forces could be produced between germline and somatic cells by flows of actomyosin linked to transmembrane E-Cad proteins, generating propelling forces. This mechanism is reminiscent of single-cell migration mechanisms used in confined or crowded environments [36–38].

Reducing contractility or adhesion specifically in germ cells induced an additional phenotype whereby germline cysts were deformed along the anterior-posterior axis and split by

ingressing somatic cells. It indicates that adhesion and contractility in germ cells regulate stiffness, which is required to sort cysts into groups of 16 cells and to resist constriction forces applied by somatic cells. The abnormal packaging of germ cells in flies with reduced adhesion or contractility in the germline is similar to the normal aggregation of germ cells from different cysts into nests that occur in mice oogenesis [3]. Our results suggest that simple differences in the regulation of cellular adhesion or cortical contractility could explain this evolutionary difference between mice and flies.

We also showed that germline cysts bleb during encapsulation. The importance of blebs for cell migration has been clearly demonstrated in several cases [39–42]. The underlying mechanisms and physical models, however, vary. One model postulates that blebs could engage in cell-cell adhesion with their environment and allow the forward transfer of cytoplasm. It has also been proposed that in a confined environment, blebs could push laterally, allowing cells to “chimney” their way forward. Our results are compatible with the role of blebs in generating propelling forces during encapsulation. The underlying physical model remains, however, to be investigated. We found that increasing bleb frequency, in *moe-TA* or *mbs-RNAi*, can induce posterior cyst migration. However, inhibiting bleb formation by expressing *moe-TD* induced only a mild reduction in bleb frequency and no significant reduction in cyst speed. It is possible that the cumulative effect of small reductions in bleb numbers, which may be below our detection methods, could nonetheless induce the observed encapsulation defects when added over several days. Our results suggest that germline cysts use migration-like mechanisms to maintain their position in the germarium during encapsulation, counterbalancing the forces exerted by ingressing FCs. These mechanisms could involve blebbing and E-Cad-based friction with the somatic layer.

Our results are a first step toward a mechanical understanding of encapsulation. Mechanical signals can instruct and pattern cell behaviors [43]. In light of our study, we can speculate that mechanical feedback between germ cells and somatic cells could play a role in self-organizing encapsulation. An important issue is to address how these mechanical inputs are integrated and regulated by biochemical signaling pathways. In both mice and flies, there is a wealth of literature describing cell-cell communications between somatic cells and between germline and somatic cells at these stages. In *Drosophila*, disruptions of the Hedgehog, Wingless, Notch, Jak/Stat, or EGF pathways lead to encapsulation defects, with the formation of compound egg chambers with multiple cysts or long stalks devoid of germ cells [44–46]. These phenotypes have been attributed mostly to defects in cell fate specifications. Our study indicates that these signaling pathways could also have a more direct role in regulating actomyosin contractility or adhesion, as their disruption induces similar defects. It will be exciting to re-analyze these biochemical and mechanical activities and their interplay during encapsulation. An integrated model of encapsulation will clearly benefit our understanding of gamete formation and reproductive biology.

STAR★METHODS

Detailed methods are provided in the online version of this paper and include the following:

- KEY RESOURCES TABLE
- RESOURCE AVAILABILITY
 - Lead Contact
 - Materials Availability
 - Data and Code Availability
- EXPERIMENTAL MODEL AND SUBJECT DETAILS
 - *Drosophila melanogaster*
- METHOD DETAILS
 - Fly stocks and genetics
 - Live and fixed imaging
 - Image processing and analysis
- QUANTIFICATION AND STATISTICAL ANALYSIS

SUPPLEMENTAL INFORMATION

Supplemental Information can be found online at <https://doi.org/10.1016/j.cub.2020.08.045>.

ACKNOWLEDGMENTS

We are grateful to Juliette Mathieu for the initial observations of germline cysts being split in *shg RNAi*. We thank A. Guichet, A.C. Martin, A. Royou, the Bloomington *Drosophila* Stock Center and the Developmental Studies Hybridoma Bank for kindly providing flies and antibodies used in this study. We thank all members of the J.-R. H. lab, F. Schweisguth, M.-E. Terret and M. Malartre for discussions and helpful comments on the manuscript. S.C. is supported by an ARC postdoctoral fellowship and work in the J.-R.H. lab is supported by CNRS, INSERM, Collège de France, La Fondation pour la Recherche Médicale (FRM) (Equipes FRM DEQ20160334884), Agence Nationale de la Recherche (ANR) (ANR-15-CE13-0001-01, AbsCyStem) and the Bettencourt Schueller Foundation.

AUTHOR CONTRIBUTIONS

Conceptualization, S.C. and J.-R.H.; Methodology, S.C. and J.-R.H.; Investigation, S.C.; Analysis, S.C.; Writing – Original Draft, S.C. and J.-R.H.; Writing – Review & Editing, S.C. and J.-R.H.; Supervision, J.-R.H.; Funding Acquisition, S.C. and J.-R.H.

DECLARATION OF INTERESTS

The authors declare no competing interests.

Received: January 17, 2020

Revised: July 1, 2020

Accepted: August 12, 2020

Published: September 10, 2020

REFERENCES

1. Pepling, M.E., de Cuevas, M., and Spradling, A.C. (1999). Germline cysts: a conserved phase of germ cell development? *Trends Cell Biol.* 9, 257–262.
2. Elkouby, Y.M., and Mullins, M.C. (2017). Coordination of cellular differentiation, polarity, mitosis and meiosis - New findings from early vertebrate oogenesis. *Dev. Biol.* 430, 275–287.
3. Lei, L., and Spradling, A.C. (2013). Mouse primordial germ cells produce cysts that partially fragment prior to meiosis. *Development* 140, 2075–2081.
4. de Cuevas, M., Lilly, M.A., and Spradling, A.C. (1997). Germline cyst formation in *Drosophila*. *Annu. Rev. Genet.* 31, 405–428.
5. Horne-Badovinac, S., and Bilder, D. (2005). Mass transit: epithelial morphogenesis in the *Drosophila* egg chamber. *Dev. Dyn.* 232, 559–574.
6. St Johnston, D., and Sanson, B. (2011). Epithelial polarity and morphogenesis. *Curr. Opin. Cell Biol.* 23, 540–546.

- Sarpal, R., Pellikka, M., Patel, R.R., Hui, F.Y., Godt, D., and Tepass, U. (2012). Mutational analysis supports a core role for *Drosophila* α -catenin in adherens junction function. *J. Cell Sci.* *125*, 233–245.
- Godt, D., and Tepass, U. (2003). Organogenesis: keeping in touch with the germ cells. *Curr. Biol.* *13*, R683–R685.
- Huynh, J.R., and St Johnston, D. (2004). The origin of asymmetry: early polarisation of the *Drosophila* germline cyst and oocyte. *Curr. Biol.* *14*, R438–R449.
- Fadiga, J., and Nystul, T.G. (2019). The follicle epithelium in the *Drosophila* ovary is maintained by a small number of stem cells. *eLife* *8*, e49050.
- Reilein, A., Melamed, D., Park, K.S., Berg, A., Cimetta, E., Tandon, N., Vunjak-Novakovic, G., Finkelstein, S., and Kalderon, D. (2017). Alternative direct stem cell derivatives defined by stem cell location and graded Wnt signalling. *Nat. Cell Biol.* *19*, 433–444.
- Morris, L.X., and Spradling, A.C. (2011). Long-term live imaging provides new insight into stem cell regulation and germline-soma coordination in the *Drosophila* ovary. *Development* *138*, 2207–2215.
- Salbreux, G., Charras, G., and Paluch, E. (2012). Actin cortex mechanics and cellular morphogenesis. *Trends Cell Biol.* *22*, 536–545.
- Lecuit, T., Lenne, P.-F., and Munro, E. (2011). Force generation, transmission, and integration during cell and tissue morphogenesis. *Annu. Rev. Cell Dev. Biol.* *27*, 157–184.
- Bendel-Stenzel, M.R., Gomperts, M., Anderson, R., Heasman, J., and Wylie, C. (2000). The role of cadherins during primordial germ cell migration and early gonad formation in the mouse. *Mech. Dev.* *91*, 143–152.
- Roubinet, C., Tsankova, A., Pham, T.T., Monnard, A., Caussinus, E., Affolter, M., and Cabernard, C. (2017). Spatio-temporally separated cortical flows and spindle geometry establish physical asymmetry in fly neural stem cells. *Nat. Commun.* *8*, 1383.
- Jaffe, A.B., and Hall, A. (2005). Rho GTPases: biochemistry and biology. *Annu. Rev. Cell Dev. Biol.* *21*, 247–269.
- Winter, C.G., Wang, B., Ballew, A., Royou, A., Karess, R., Axelrod, J.D., and Luo, L. (2001). *Drosophila* Rho-associated kinase (Drok) links Frizzled-mediated planar cell polarity signaling to the actin cytoskeleton. *Cell* *105*, 81–91.
- Burnett, K., Edsinger, E., and Albrecht, D.R. (2018). Rapid and gentle hydrogel encapsulation of living organisms enables long-term microscopy over multiple hours. *Commun. Biol.* *1*, 73.
- Diz-Muñoz, A., Fletcher, D.A., and Weiner, O.D. (2013). Use the force: membrane tension as an organizer of cell shape and motility. *Trends Cell Biol.* *23*, 47–53.
- Charras, G., and Paluch, E. (2008). Blebs lead the way: how to migrate without lamellipodia. *Nat. Rev. Mol. Cell Biol.* *9*, 730–736.
- Hawkins, N.C., Thorpe, J., and Schüpbach, T. (1996). Encore, a gene required for the regulation of germ line mitosis and oocyte differentiation during *Drosophila* oogenesis. *Development* *122*, 281–290.
- Mathieu, J., Cauvin, C., Moch, C., Radford, S.J., Sampaio, P., Perdigo, C.N., Schweisguth, F., Bardin, A.J., Sunkel, C.E., McKim, K., et al. (2013). Aurora B and cyclin B have opposite effects on the timing of cytokinesis abscission in *Drosophila* germ cells and in vertebrate somatic cells. *Dev. Cell* *26*, 250–265.
- Godt, D., and Tepass, U. (1998). *Drosophila* oocyte localization is mediated by differential cadherin-based adhesion. *Nature* *395*, 387–391.
- González-Reyes, A., and St Johnston, D. (1998). The *Drosophila* AP axis is polarised by the cadherin-mediated positioning of the oocyte. *Development* *125*, 3635–3644.
- Fichelson, P., Jagut, M., Lepanse, S., Lepesant, J.A., and Huynh, J.R. (2010). Lethal giant larvae is required with the par genes for the early polarization of the *Drosophila* oocyte. *Development* *137*, 815–824.
- Peifer, M., Orsulic, S., Sweeton, D., and Wieschaus, E. (1993). A role for the *Drosophila* segment polarity gene armadillo in cell adhesion and cytoskeletal integrity during oogenesis. *Development* *118*, 1191–1207.
- White, P., Aberle, H., and Vincent, J.P. (1998). Signaling and adhesion activities of mammalian beta-catenin and plakoglobin in *Drosophila*. *J. Cell Biol.* *140*, 183–195.
- Kunda, P., Pelling, A.E., Liu, T., and Baum, B. (2008). Moesin controls cortical rigidity, cell rounding, and spindle morphogenesis during mitosis. *Curr. Biol.* *18*, 91–101.
- Maitre, J.-L., Niwayama, R., Turlier, H., Nédélec, F., and Hiiragi, T. (2015). Pulsatile cell-autonomous contractility drives compaction in the mouse embryo. *Nat. Cell Biol.* *17*, 849–855.
- Weiner, O.D., Marganski, W.A., Wu, L.F., Altschuler, S.J., and Kirschner, M.W. (2007). An actin-based wave generator organizes cell motility. *PLOS Biol.* *5*, e221.
- Bement, W.M., Leda, M., Moe, A.M., Kita, A.M., Larson, M.E., Golding, A.E., Pfeuti, C., Su, K.C., Miller, A.L., Goryachev, A.B., and von Dassow, G. (2015). Activator-inhibitor coupling between Rho signalling and actin assembly makes the cell cortex an excitable medium. *Nat. Cell Biol.* *17*, 1471–1483.
- Cavey, M., Rauzi, M., Lenne, P.-F., and Lecuit, T. (2008). A two-tiered mechanism for stabilization and immobilization of E-cadherin. *Nature* *453*, 751–756.
- Yonemura, S., Wada, Y., Watanabe, T., Nagafuchi, A., and Shibata, M. (2010). α -Catenin as a tension transducer that induces adherens junction development. *Nat. Cell Biol.* *12*, 533–542.
- Liu, Z., Tan, J.L., Cohen, D.M., Yang, M.T., Sniadecki, N.J., Ruiz, S.A., Nelson, C.M., and Chen, C.S. (2010). Mechanical tugging force regulates the size of cell-cell junctions. *Proc. Natl. Acad. Sci. USA* *107*, 9944–9949.
- Bergert, M., Erzberger, A., Desai, R.A., Aspalter, I.M., Oates, A.C., Charras, G., Salbreux, G., and Paluch, E.K. (2015). Force transmission during adhesion-independent migration. *Nat. Cell Biol.* *17*, 524–529.
- Hawkins, R.J., Poincloux, R., Bénichou, O., Piel, M., Chavrier, P., and Voituriez, R. (2011). Spontaneous contractility-mediated cortical flow generates cell migration in three-dimensional environments. *Biophys. J.* *101*, 1041–1045.
- Paluch, E.K., Aspalter, I.M., and Sixt, M. (2016). Focal Adhesion-Independent Cell Migration. *Annu. Rev. Cell Dev. Biol.* *32*, 469–490.
- Paluch, E.K., and Raz, E. (2013). The role and regulation of blebs in cell migration. *Curr. Opin. Cell Biol.* *25*, 582–590.
- Paluch, E., Sykes, C., Prost, J., and Bornens, M. (2006). Dynamic modes of the cortical actomyosin gel during cell locomotion and division. *Trends Cell Biol.* *16*, 5–10.
- Ruprecht, V., Wieser, S., Callan-Jones, A., Smutny, M., Morita, H., Sako, K., Barone, V., Ritsch-Marte, M., Sixt, M., Voituriez, R., and Heisenberg, C.P. (2015). Cortical contractility triggers a stochastic switch to fast amoeboid cell motility. *Cell* *160*, 673–685.
- Liu, Y.-J., Le Berre, M., Lautenschlaeger, F., Maiuri, P., Callan-Jones, A., Heuzé, M., Takaki, T., Voituriez, R., and Piel, M. (2015). Confinement and low adhesion induce fast amoeboid migration of slow mesenchymal cells. *Cell* *160*, 659–672.
- Chanet, S., and Martin, A.C. (2014). Mechanical force sensing in tissues. *Prog. Mol. Biol. Transl. Sci.* *126*, 317–352.
- Bastock, R., and St Johnston, D. (2008). *Drosophila* oogenesis. *Curr. Biol.* *18*, R1082–R1087.
- Klusza, S., and Deng, W.M. (2011). At the crossroads of differentiation and proliferation: precise control of cell-cycle changes by multiple signaling pathways in *Drosophila* follicle cells. *BioEssays* *33*, 124–134.
- Roth, S., and Lynch, J.A. (2009). Symmetry breaking during *Drosophila* oogenesis. *Cold Spring Harb. Perspect. Biol.* *1*, a001891.
- Royou, A., Sullivan, W., and Karess, R. (2002). Cortical recruitment of non-muscle myosin II in early syncytial *Drosophila* embryos: its role in nuclear axial expansion and its regulation by Cdc2 activity. *J. Cell Biol.* *158*, 127–137.
- Martin, A.C., Kaschube, M., and Wieschaus, E.F. (2009). Pulsed contractions of an actin-myosin network drive apical constriction. *Nature* *457*, 495–499.

49. Rauzi, M., Lenne, P.F., and Lecuit, T. (2010). Planar polarized actomyosin contractile flows control epithelial junction remodelling. *Nature* **468**, 1110–1114.
50. Huelsmann, S., Yläanne, J., and Brown, N.H. (2013). Filopodia-like actin cables position nuclei in association with perinuclear actin in *Drosophila* nurse cells. *Dev. Cell* **26**, 604–615.
51. Bardet, P.-L., Guirao, B., Paoletti, C., Serman, F., Léopold, V., Bosveld, F., Goya, Y., Mirouse, V., Graner, F., and Bellaïche, Y. (2013). PTEN controls junction lengthening and stability during cell rearrangement in epithelial tissue. *Dev. Cell* **25**, 534–546.
52. Huang, J., Zhou, W., Dong, W., Watson, A.M., and Hong, Y. (2009). From the Cover: Directed, efficient, and versatile modifications of the *Drosophila* genome by genomic engineering. *Proc. Natl. Acad. Sci. USA* **106**, 8284–8289.
53. Morin, X., Daneman, R., Zavortink, M., and Chia, W. (2001). A protein trap strategy to detect GFP-tagged proteins expressed from their endogenous loci in *Drosophila*. *Proc. Natl. Acad. Sci. USA* **98**, 15050–15055.
54. Van Doren, M., Williamson, A.L., and Lehmann, R. (1998). Regulation of zygotic gene expression in *Drosophila* primordial germ cells. *Curr. Biol.* **8**, 243–246.
55. Clémot, M., Molla-Herman, A., Mathieu, J., Huynh, J.R., and Dostatni, N. (2018). The replicative histone chaperone CAF1 is essential for the maintenance of identity and genome integrity in adult stem cells. *Development* **145**, dev161190.
56. Vasquez, C.G., Tworoger, M., and Martin, A.C. (2014). Dynamic myosin phosphorylation regulates contractile pulses and tissue integrity during epithelial morphogenesis. *J. Cell Biol.* **206**, 435–450.
57. Loyer, N., Kolotuev, I., Pinot, M., and Le Borgne, R. (2015). *Drosophila* E-cadherin is required for the maintenance of ring canals anchoring to mechanically withstand tissue growth. *Proc. Natl. Acad. Sci. USA* **112**, 12717–12722.

STAR★METHODS

KEY RESOURCES TABLE

REAGENT or RESOURCE	SOURCE	IDENTIFIER
Antibodies		
Mouse anti-Orb 4H8 (1:500)	DSHB	RRID: AB_528418
Rat anti-DE-Cadherin2 (1:50)	DSHB	RRID: AB_528120
Rat anti-DN-Cadherin (1:25)	DSHB	RRID: AB_528121
Chemicals, Peptides, and Recombinant Proteins		
Phalloidin Alexa Fluor 568	Invitrogen	Cat # A12380
DAPI	Invitrogen	Cat # D1306
Y-27632 (ROCK inhibitor)	Enzo Life Sciences	CAS # 129830-38-2 Cat # ALX270333M001
DMSO	Sigma	Cat # D2650
Cyto-D	Enzo Life Sciences	CAS # 22144-77-0 Cat # BML-T109-0001
CK-666	Sigma	CAS # 442633-00-3 Cat # SML0006
Colcemid	Sigma	CAS # 477-30-5 Cat # 10295892001
3-(trimethoxysilyl)propyl methacrylate	Sigma	CAS # 2530-85-0 Cat # 440159
PEG-DA	Esibio	Cat # GS700
Irgacure 2959	Sigma	CAS # 106797-53-9 Cat # 410896
Experimental Models: Organisms/Strains		
sqh ^{AX3} ; sqh::GFP	R. Karress	[47]
sqh ^{AX3} ; sqh::mCherry	A. C. Martin	[48]
w;; Utr::GFP	T. Lecuit	[49]
w; UASp-LifeAct::GFP	BDSC	[50]
ubip-GFP::ROCK	Y. Bellaïche	[51]
ECad::GFP ^{K1}	H. Yang	[52]
arm::GFP	BDSC	#8556
Jupiter::GFP	BDSC	[53]
w; sqh::Dendra2	A. Royou	[16]
v;; UASp-white-shRNA	BDSC	#35573
v;; UASp-chic-shRNA	BDSC	#34523
v; UASp-zip-shRNA	BDSC	#37480
v; UASp-mbs-shRNA	BDSC	#41625
v; UASp-shg-shRNA	BDSC	#38207
v; UASp-arm-shRNA	BDSC	#35004
w; sqh::GFP; UASp-chic-shRNA	This study	from stocks BDSC #34523 and [47]
w; UASp-zip-shRNA; Utr::GFP	This study	from stocks BDSC #37480 and [49]
w; UASp-mbs-shRNA; Utr::GFP	This study	from stocks BDSC #41625 and [49]
w;; nanos-GAL4-VP16 (nos-GAL4)	BDSC	[54]
w; sqh::GFP; nos-GAL4	This study	from [47] and [54]
w; UASp-GFP; nos-GAL4	This study	N/A
w; bam-GAL4(x2)	J. Mathieu	[55]
w; bam-GAL4(x2); Utr::GFP	This study	from [55] and [49]
w; Traffic jam-GAL4; Utr::GFP	This study	from stocks BDSC # 50105 and [49]

(Continued on next page)

Continued

REAGENT or RESOURCE	SOURCE	IDENTIFIER
w hs-Flp; UASp-GFP; act-FRT-y+-FRT-GAL4	This study	From stock BDSC # 30558
w FRT-19A rok ²	BDSC	[18]
w hs-Flp FRT-19A ubi-mRFP.nls	BDSC	# 31418
w FRT ¹⁰¹ sqh ¹	C. Vasquez	[56]
w hs-Flp FRT ¹⁰¹ ubi-GFP	C. Vasquez	from #5153 and [56]
w; FRT[G13-42B], shg ^{R69} / CyO	R. Le Borgne	[57]
y w hs-FLP; FRT[G13-42B] Ubi-nls::GFP / CyO	R. Le Borgne	[57]
w; UASp-moe-TA::GFP	A. Guichet	N/A
w; UASp-moe-TD::GFP	A. Guichet	N/A
w; UASp-moe-TA::GFP; Utr::GFP	This study	N/A
w; UASp-moe-TD::GFP; Utr::GFP	This study	N/A
w; UASp-moe-TA::GFP; sqh::mCherry	This study	N/A
w; UASp-moe-TD::GFP; sqh::mCherry	This study	N/A
Software and Algorithms		
Fiji	NIH	http://fiji.sc/
PRISM 8	GraphPad	https://www.graphpad.com/scientific-software/prism/
Imaris Bitplane	Oxford Instruments	https://imaris.oxinst.com

DSHB: Developmental Studies Hybridoma Bank; BDSC, Bloomington Drosophila Stock Center.

RESOURCE AVAILABILITY

Lead Contact

Further information and requests for resources and reagents should be directed to and will be fulfilled by the Lead Contact, Jean-René Huynh (jean-rene.huynh@college-de-france.fr).

Materials Availability

This study did not generate new unique reagents.

Data and Code Availability

The datasets supporting the current study have not been deposited in a public repository but are available from the corresponding author on request.

EXPERIMENTAL MODEL AND SUBJECT DETAILS

Drosophila melanogaster

Flies were maintained on standard medium in 25°C incubators on a 12 h light/dark cycle. Wild-type controls were from w¹¹¹⁸ background flies with additional transgenes of fluorescently tagged proteins. The white-shRNA was used as a control for knock-down experiments (*ctl-RNAi*) because *white* is not expressed during oogenesis.

METHOD DETAILS

Fly stocks and genetics

Myosin was visualized in live germlaria using myosin regulatory light chain (*sqh* in *Drosophila*) fused to GFP or mCherry expressed under its own promoter. Actin was visualized using the F-actin binding domain of Utrophin fused to GFP (Utr::GFP) expressed under an ubiquitous promoter (*sqh* promoter) or using the UASp-LifeAct::GFP construct expressed in the germline using the nanos-GAL4-VP16 (*nos-GAL4*) driver. To visualize ROCK in live, we used a wild-type ROCK allele fused to GFP expressed under an ubiquitous promoter. To visualize E-Cad in live, we used a knock-in insertion of GFP at the DE-Cad locus. Microtubules were visualized in live using the microtubule-associated protein Jupiter fused to GFP.

Depending on the strength of the shRNA, different drivers were used for knockdowns in the germline. To knockdown *zip* and *mbs* we used *nos-GAL4*. To knockdown *chic* and *shg* we used a *bam-GAL4(x2)* driver (containing two copies of the

bam-GAL4 driver). For gene knockdowns in follicle cells, we used Traffic jam-GAL4 driver. Knock downs were performed at 29°C to increase the efficiency of the GAL4 driver.

To generate Flp out clones we used the stock: w^{hs}-Flp; UASp-GFP; act-FRT-y⁺-FRT-GAL4 (generated using stocks from BDSC). Heat-shocks were performed on early pupae, 30 min at 37°C.

*rok*² and *shq*¹ clones were generated using the Flp/FRT technique. To induce clones, heat-shocks were performed on L2 larvae for 1h at 37°C for two consecutive days.

To modify cortex properties, favoring or reducing blebs occurrences, we expressed tagged version of Moesin in the germline using the nos-GAL4 driver. w; UASp-moe-TA::GFP, w; UASp-moe-TD::GFP are gifts from A. Guichet. Crosses were kept at 29°C to increase the efficiency of the GAL4 driver.

Live and fixed imaging

5-day-old females were collected and dissected for live imaging or fixed experiments.

Live imaging in hydrogel was adapted from Burnett et al. [19]. Ovaries were dissected in Schneider medium (Sigma-Aldrich), and transferred onto a round 25 mm coverslip. The coverslips were previously coated with 3-(trimethoxysilyl)propyl methacrylate (Sigma-Aldrich). Medium was removed and 15 μ L of 10% PEG-DA hydrogel solution (esibio) with 0.1% I2959 (photo initiator, Sigma-Aldrich) was added on the samples. A coverslip treated with deperlent was placed over the hydrogel droplet and the coverslip/coverslip sandwich was then placed over a UV light source and illuminated for 30 s at 312nm for gelation. The upper coverslip was removed and the coverslip supporting the hydrogel disc was then placed into a chamber (Chamlide) filled with Schneider medium. See [Figure S1B](#). All imaging was performed at 25°C.

Drugs treatment. Few microliters of chemical or vehicle were added directly to the culture chamber while imaging. Cyto-D (Enzo Life Sciences) and CK-666 (Sigma) were diluted in DMSO (Sigma). Final concentrations in Schneider medium after addition of the drugs to the culture chamber were 2.5 μ M for Cyto-D and 50 μ M for CK-666. Y27632 (Enzo Life Sciences) was diluted in water and added to the chamber for a final concentration of 500 μ M. Colcemid (Sigma) was added for a final concentration of 62 μ g.mL⁻¹.

For live imaging in oil, ovaries were dissected in oil (10S, Voltalef, VWR) and transferred onto a coverslip. Germaria were made to stick to the coverslip in oil.

For immunostaining, ovaries were dissected in PBS, fixed in 4%PFA, permeabilized in PBT (0.2%Triton) for 30 min, left overnight with primary antibodies in PBT at 4°C, washed 3 times 30 min in PBT, left with secondary antibody for 2 h at room temperature, washed 3 times 30 min in PBT and mounted in Citifluor. All images were acquired on an inverted spinning-disc confocal microscope (Roper/Nikon) operated by Metamorph 7.7 coupled to a sCMOS camera and with a 60X/1.4 oil objective.

Image processing and analysis

Images were processed using Fiji and Imaris (Bitplane) and graphs were generated in Prism (GraphPad). A bleach correction was applied to time-lapse images. Images of the movies represent a maximum intensity Z projection (20 μ m).

Waves and blebs occurrences were measured in Fiji using movies recorded at a rate of 30 s per z stack (20 slices, representing 20 μ m). A wave was defined as a bright myosin accumulation (we either used *sqh-GFP*, [Figures 1](#) and [2](#), [Figure S2](#) or *sqh-mCherry*, [Figure S4](#)) that was moving around the cortex before dissociation, we did not consider as wave bright spots of cortical or junctional myosin that were static or moving very slowly. We noticed that waves could run around the cortex in any direction in 3D, thus, to perform our analysis we used maximum projections of stacks of 20 μ m. Wave occurrences were either counted per cell ([Figure 1F](#)) or per cysts ([Figures 1I](#), [2B](#), [4G](#), [S2A](#), and [S4A](#)).

A bleb was defined as spherical expanding and retracting protrusion. To follow bleb dynamics, we expressed a cytoplasmic GFP (UASp-GFP) in the germline in the different conditions analyzed. Note that blebs were counted on maximum projections of stacks of 20 μ m, such that bleb number was underestimated (blebs forming perpendicular to the plan of view were not visible and not counted). We either quantify bleb frequency ([Figure 1K](#)) or the average number of blebs per cyst ([Figures 5](#) and [S2C](#)). To do so, we counted the number of blebs per cyst for each time frame (every 30 s) and divided by the number of frames. This method was used to take into account bleb persistence.

Region 3 cyst aspect ratios ([Figures 3](#) and [S4B](#)) were measured in Fiji using the build-in toolbox, an ellipse was fitted to the shape of the cyst (as indicated in [Figure 3F](#)).

Cyst displacement were tracked in Imaris. Movies were recorded at a rate of 3 to 5 min per z stack (20 slices, representing 20 μ m) for 1 to 2 h. Cap cells at the anterior tip of the germarium were used as a fixed reference point. To estimate cyst displacement, we tracked the oldest ring canal of each cyst, which is the widest and brightest, making it an easy object to track. We projected displacement along the a-p axis using Imaris build-in toolbox and calculated the mean speed over 1 to 2 h. By convention, we conferred a negative value for displacement speed toward the anterior and a positive value for displacement speed toward the posterior.

To calculate the percentage of stalk width reduction over 50 min in hydrogel versus in oil, we measure the width of the stalk at t = 0 and at t = 50 min and divided the difference by the initial width.

QUANTIFICATION AND STATISTICAL ANALYSIS

Statistical analyses were performed using the Prism (Graphpad) statistics toolbox. For waves and blebs frequency as well as for aspect ratio, *P* values were calculated using an unpaired t test, the reference sample is the distribution in wild-type.

Figure 1F: n = 6 GSC or Cystoblast, n = 12 cells of 2-cell cysts, n = 21 cells of 4-cell cysts, n = 33 cells of 8-cell cysts, n = 61 cells of region 2a cysts, n = 45 cells of region 2b cysts, n = 42 cells of region 3 cysts; 4 germlaria.

Figure 1K: n = 19 region 2b cysts, n = 13 region 3 cysts, 19 germlaria.

Figure 2B: n = 5 cysts in region 2a, n = 8 cysts in region 2b, n = 8 cysts in region 3, 5 *ctl-RNAi* germlaria; n = 5 cysts in region 2a, n = 4 cysts in region 2b, n = 5 cysts in region 3, 5 *chic-RNAi* germlaria; n = 4 cysts in region 2a, n = 6 cysts in region 2b, n = 5 cysts in region 3, 3 *zip-RNAi* germlaria; n = 5 cysts in region 2a, n = 9 cysts in region 2b, n = 7 cysts in region 3, 5 *mbs-RNAi* germlaria.

Figure 3B: n = 26 *ctl-RNAi*, n = 30 *chic-RNAi*, n = 25 *zip-RNAi*, n = 38 *mbs-RNAi*.

Figure 4D: n = 26 *ctl-RNAi*, n = 33 *ECad-RNAi* germ, n = 17 *ECad-RNAi* soma.

Figure 4G: n = 6 cysts in region 2a, n = 8 cysts in region 2b, n = 6 cysts in region 3, 5 *ECad-RNAi* germlaria.

Figure 4I: n = 11 cysts in region 2b, n = 13 cysts in region 3, 16 wild-type germlaria; n = 11 cysts in region 2b, n = 10 cysts in region 3, 9 *ECad-RNAi* germlaria.

Figure 5B: n = 11 cysts in region 2b, n = 13 cysts in region 3, 16 wild-type germlaria; n = 12 cysts in region 2b, n = 27 cysts in region 3, 20 *moe-TA::GFP* germlaria, n = 8 cysts in region 2b, n = 11 cysts in region 3, 10 *moe-TD::GFP* germlaria.

To compare cysts displacements speed in our different conditions, we used a non-parametric Mann-Whitney *U*-test. the reference sample is the distribution in *ctl-RNAi*. Statistical analyses were performed on absolute value of cyst displacement speed.

Figure 3B: n = 20 cysts in region 2b, 24 cysts in region 3 for *ctl-RNAi*; n = 25 cysts in region 2b, 31 cysts in region 3 for *chic-RNAi*; n = 21 cysts in region 2b, 33 cysts in region 3 for *zip-RNAi*; n = 21 cysts in region 2b, 42 cysts in region 3 for *mbs-RNAi*.

Figure 4E: n = 25 cysts in region 2b, 28 cysts in region 3 for *shg-RNAi* germ.; n = 17 cysts in region 2b, 22 cysts in region 3 for *shg-RNAi* soma.

Figure 5E: n = 21 cysts in region 3 for *moe-TA::GFP*; n = 12 cysts in region 3 for *moe-TD::GFP*.

To compare constriction of the stalk in hydrogel versus oil, *P* value was calculated using an unpaired t test, the reference sample is the distribution in hydrogel.

Figure 6A: n = 20 germlaria mounted in hydrogel, n = 13 germlaria mounted in oil.

Cysts autonomous migration on stalled FCs (**Figures 6B** and **S5B**) was tested using a non-parametric one sample Wilcoxon test. *P* values were calculated against the null hypothesis $m = 0$ (no displacement).

Figure 6B: n = 26 cyst in region 3 *ctl-RNAi*; 25 cysts in region 3 for *zip-RNAi*, 22 cysts in region 3 for *shg-RNAi*.